

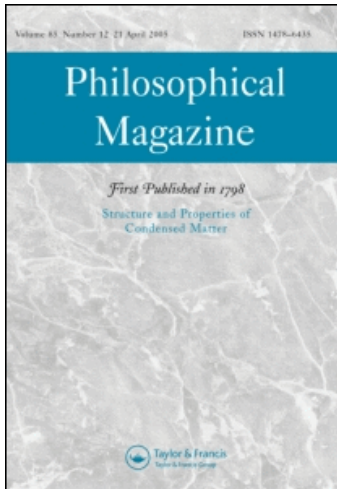
This article was downloaded by: [CAS Chinese Academy of Sciences]

On: 14 July 2009

Access details: Access Details: [subscription number 906076485]

Publisher Taylor & Francis

Informa Ltd Registered in England and Wales Registered Number: 1072954 Registered office: Mortimer House, 37-41 Mortimer Street, London W1T 3JH, UK



Philosophical Magazine

Publication details, including instructions for authors and subscription information:

<http://www.informaworld.com/smpp/title~content=t713695589>

Cyclic deformation and fatigue cracking behaviors of Cu-28wt%Ag binary alloy

Y. Z. Tian ^a; Z. F. Zhang ^a; Z. G. Wang ^a

^a Shenyang National Laboratory for Materials Science, Institute of Metal Research, Shenyang 110016, China

Online Publication Date: 01 July 2009

To cite this Article Tian, Y. Z., Zhang, Z. F. and Wang, Z. G. (2009) 'Cyclic deformation and fatigue cracking behaviors of Cu-28wt%Ag binary alloy', *Philosophical Magazine*, 89:21, 1715 — 1730

To link to this Article: DOI: 10.1080/14786430903032548

URL: <http://dx.doi.org/10.1080/14786430903032548>

PLEASE SCROLL DOWN FOR ARTICLE

Full terms and conditions of use: <http://www.informaworld.com/terms-and-conditions-of-access.pdf>

This article may be used for research, teaching and private study purposes. Any substantial or systematic reproduction, re-distribution, re-selling, loan or sub-licensing, systematic supply or distribution in any form to anyone is expressly forbidden.

The publisher does not give any warranty express or implied or make any representation that the contents will be complete or accurate or up to date. The accuracy of any instructions, formulae and drug doses should be independently verified with primary sources. The publisher shall not be liable for any loss, actions, claims, proceedings, demand or costs or damages whatsoever or howsoever caused arising directly or indirectly in connection with or arising out of the use of this material.

Cyclic deformation and fatigue cracking behaviors of Cu–28wt%Ag binary alloy

Y.Z. Tian, Z.F. Zhang* and Z.G. Wang

*Shenyang National Laboratory for Materials Science, Institute of Metal Research,
Chinese Academy of Sciences, 72 Wenhua Road, Shenyang 110016, China*

(Received 7 December 2008; final version received 9 May 2009)

The cyclic deformation and fatigue cracking behaviors of coarse-grained Cu–28wt%Ag binary alloy were investigated under axial plastic strain amplitudes ranging from 10^{-4} to 7.5×10^{-4} . It was found that the cyclic stress of the Cu–Ag alloy increased rapidly in the initial tens of cycles and became saturation with further cyclic deformation. The cyclic saturation stress increased with increasing the plastic strain amplitude. The interfaces are classified into two categories based on the orientations of the eutectic and the dendrites, i.e. type I and type II interfaces. The surface damage morphologies show that fatigue cracks normally nucleated either along the type I interfaces or along the slip bands (SBs), while no cracking occurred along the type II interface. Fatigue striations with different spacings appeared on the fracture surface, and secondary cracks along the striations were also observed. Based on the experimental results, the cyclic deformation and fatigue cracking behavior of the Cu–Ag binary alloy were discussed in detail.

Keywords: Cu–Ag alloy; cyclic deformation; slip bands; fatigue cracking; interphase interface; fatigue striation

1. Introduction

It is well known that fatigue damage or cracking is important in engineering materials. Ewing and Humfrey [1] first reported the fatigue damage behavior of polycrystalline Swedish iron subjected to repeated reversal of stress by bending at room temperature in air. Since the 1950s, much attention has been paid to the fatigue properties of various crystalline materials. Fatigue cracking behavior associated with persistent slip bands (PSBs) in various single crystals has been widely investigated [2]. For example, Finney and Laird [3] and Cheng and Laird [4] measured the surface slip steps induced by PSBs during fatigue of Cu single crystals using an optical interference technique. Polák and coworkers [5,6] investigated fatigue crack initiation in PSBs by introducing a point-defect approach. Lukáš et al. [7] provided several prerequisites for micro-crack initiation, while Brown [8] investigated dislocation plasticity in PSBs. Basinski and Basinski [9–12] found that not all the intrusions induced by PSBs led to fatigue cracks; furthermore, they defined fatigue

*Corresponding author. Email: zhfzhang@imr.ac.cn

cracks as intrusions that grew continuously to a critical height of 3–4 μm . Hunsche and Neumann [13] investigated the fatigue cracking mechanism along PSBs using a sharp-corner cutting technique. In addition, Essmann et al. [14–16] postulated some theoretical explanations for fatigue cracking along PSBs based on point-defect production and growth of extrusions as well as surface roughening by irreversible slip.

Observations on fatigue cracking and the cracking mechanisms in polycrystalline materials have also received much attention over the last 30 years. Figueroa and Laird [17] and Mughrabi and Wang [18] found that fatigue cracks often nucleated along GBs in polycrystalline Cu at intermediate strain amplitudes. In contrast, Cooper and Fine [19] found that PSBs were still the preferential sites for fatigue crack initiation. It was also reported that the loading modes play a significant role in the fatigue cracking mechanism. For example, Kim et al. [20] found that fatigue cracks in polycrystalline Cu mainly initiated along PSBs under cyclic push–pull loading; however, under cyclic tension–tension loading, GBs often became the preferential sites for the induction of fatigue cracks. Thus, fatigue cracking is always associated with plastic strain localization, for example, at the interface between PSBs and the matrix and GBs. Based on experiments, Kim and Laird [21,22] proposed a step mechanism to explain the fatigue cracking at high plastic strain amplitudes. On the other hand, Mughrabi et al. [23] proposed another mechanism based on the interaction between PSBs and GBs in polycrystalline Cu by taking account of the piling-up of dislocations at GBs due to irreversible slip during cyclic deformation. Recently, Zhang et al. [24–29] concentrated on the effect of GBs on fatigue damage by employing bicrystals with high-angle, low-angle and special GBs using a electron channel contrast (ECC) technique in a scanning electron microscope (SEM). Moreover, high-resolution technique, such as atomic force microscope (AFM) and three-dimension discrete dislocation dynamics modeling, represent new tools for the study of fatigue crack initiation [30–34].

However, most of the studies mentioned above mainly concentrated on single-phase crystalline materials. In two-phase materials, the fatigue crack nucleation sites depend on the microstructures and mechanical properties of both phases and their responses to cyclic deformation [35–36]. In many alloys, such as hypoeutectic Al–Si binary alloy, alpha/beta titanium alloys and duplex stainless steel, the short crack nucleation was along the interphase interfaces [35–42], and the internal stresses associated with strain incompatibility may be the origin of crack initiation. Pineau et al. [43,44] carried out numerous tests on the fatigue and creep properties of various steels. Recently, some Cu–Ag binary alloys with high strength and good conductivity have been developed by cold-rolling or drawing [45–47]. Such *in situ* Cu–Ag composites can be used to fabricate high field magnets [48–50] or utilized in engineering applications as a structural material. However, research on the fatigue properties of Cu–Ag binary alloy, especially the fatigue damage mechanism, is rare [51]. In addition, Cu–Ag binary alloy can be considered as a model material to reveal the fundamental fatigue damage mechanism. Based on our systematic investigations of fatigue damage mechanisms of single crystals, bicrystals, Cu–Al and Cu–Zn alloys [24–29,52,53], we will continue to focus on the fatigue damage behavior of the Cu–Ag binary alloy. In coarse-grained hypoeutectic Cu–16wt%Ag

binary alloy, the eutectic often shows the same orientation or low-angle misorientation as the Cu dendrites, and the SBs can pass continuously through the interfaces between them, which could be attributed to coplanar slip systems near the interfaces [54]. This case gives rise to an interesting question: what are the cracking sites when applying cyclic deformation to the Cu–Ag binary alloy? In this paper, a Cu–28wt%Ag binary alloy is employed to reveal the cyclic stress–strain responses and fatigue cracking mechanisms in more detail.

2. Experimental procedures

The starting materials were OFHC Cu of 99.999% purity and electrolytic Ag of 99.99% purity. A Cu–28wt%Ag alloy plate with dimensions of $40 \times 15 \times 150$ mm was molten at a temperature of 1200°C by the Bridgman method using a graphite crucible in a horizontal furnace. The slow cooling rate made the microstructure much coarser and more in equilibrium; therefore, the annealing process was excluded to maintain the as-cast microstructure and facilitate investigation of the microscopic fatigue damage mechanism.

Since Cu–28wt%Ag is a hypoeutectic alloy containing Ag- and Cu-rich phases, the difference in electro-polishing rate results in difficulty in sample preparation. Thus, an ion-milling method was conducted for electron backscattered diffraction (EBSD) mapping of the alloy [55]. A slice of the alloy was initially ground and polished to a thickness less than $200\ \mu\text{m}$; then, samples of 3 mm in diameter were punched for ion milling. Ion-milling conditions were as reported previously [54]. Finally, the samples were observed with a LEO Supra 35 field-emission scanning electron microscope (FE-SEM) equipped with an EBSD system.

The fatigue specimens with gauge dimensions of $16 \times 5 \times 4$ mm and a total length of 60 mm were machined by a spark-cutting technique. Before fatigue testing, all the specimens were ground and mechanically polished carefully for surface observation. Then, they were cyclically deformed in push–pull on a Shimadzu servo-hydraulic testing machine under constant plastic strain amplitude control at room temperature in air. Under axial plastic strain amplitudes of $\varepsilon_{pl} = 10^{-4}$, 2.5×10^{-4} , 5×10^{-4} and 7.5×10^{-4} , the specimens were cyclically deformed to 2×10^4 , 1.5×10^4 , 10^4 and 5×10^3 cycles, respectively. To reveal the fracture surface, some specimens were selected for further cyclic loading to failure. The surface deformation morphologies and fatigue fractographs of the specimens were then observed by a LEO Supra 35 SEM.

3. Experimental results

3.1. Microstructure observation

Figures 1a and b show the SEM backscattered diffraction image and the Kikuchi band contrast and high-angle boundary map. The high-angle boundaries are shown in Figure 1b, with the black lines representing the boundaries with misorientation angle greater than 15° . Large areas of the preeutectic region have the same orientation, indicating that they belong to the same dendrite, whereas the eutectic has the same orientation or low misorientation angle ($< 15^\circ$) with the dendrites,

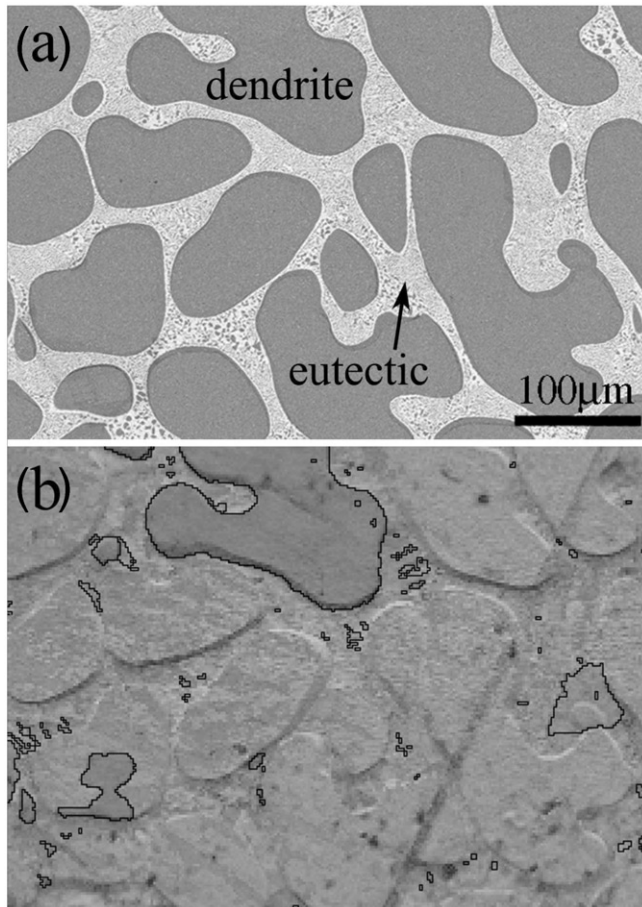


Figure 1. Microstructures of Cu-28wt%Ag alloy. (a) SEM backscattered diffraction image. (b) Kikuchi band contrast and high-angle boundary map of the same area.

which is believed to be the result of nucleation on the dendrite [54]. Furthermore, some regions with different orientations appear inside the eutectic (see Figure 1b). In contrast to the Cu-16wt%Ag alloy [54], such regions are distributed more widely; thus, in the current study, the eutectic is more disordered. A detailed description and discussion on the microstructure of coarse-grained Cu-Ag alloy is available elsewhere [54]. Note that the alloy contains a large number of interfaces; however, they can be classified into two categories based on the orientation of the eutectic and dendrites: type I and type II interfaces. Near the type I interfaces, the eutectic and dendrites have high misorientation angles ($\geq 15^\circ$), whereas they have the same orientation or low misorientation angles ($< 15^\circ$) near type II interfaces. The complex microstructure of the Cu-28wt%Ag alloy may have a significant effect on the slip deformation process during cyclic deformation. This will be analyzed in the following sections by observing the surface deformation morphology.

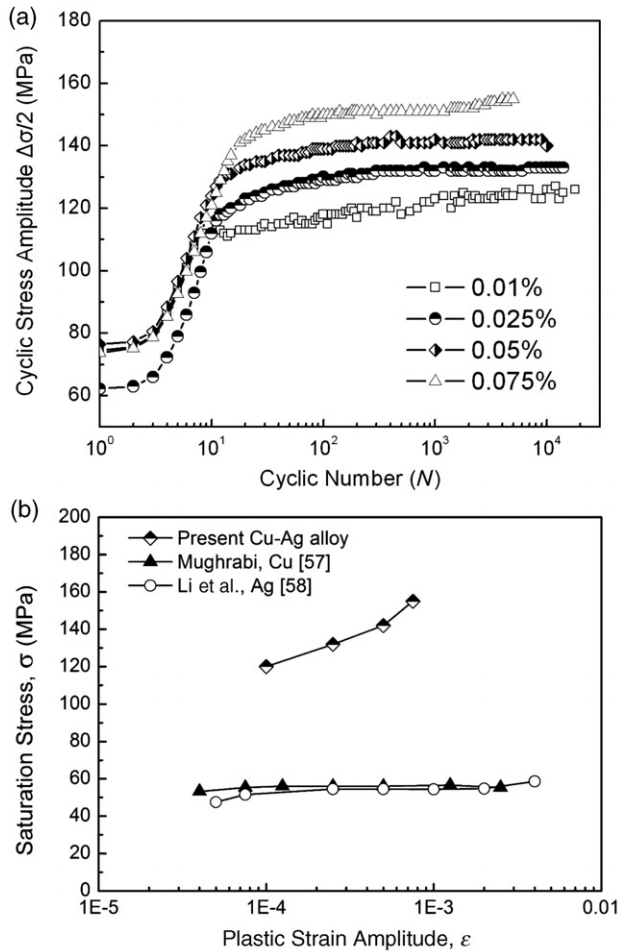


Figure 2. (a) Cyclic hardening curves of Cu–28wt%Ag alloy under several plastic strain amplitudes. (b) Cyclic stress–strain curve of Cu–28wt%Ag alloy, coupled with the CSS curves of Cu and Ag single crystals orientated for single slip [42,43].

3.2. Cyclic hardening and saturation

In view of the complex microstructures of the Cu–28wt%Ag alloy, its fatigue properties were tested and elucidated. Figure 2a shows the cyclic hardening curves under several axial plastic strain amplitudes. After only ~ 50 cycles, all the samples were nearly saturated, showing a faster cyclic saturation process than pure Cu or Ag single crystals or Cu polycrystals [24,53,56]. When $\epsilon_{pl} = 10^{-4}$, cyclic saturation is nearly achieved within 10 cycles. The cyclic stress–strain (CSS) curve of Cu–Ag alloy is shown in Figure 2b, coupled with the CSS curves of Cu and Ag single crystals orientated for single slip [57,58]. Both Cu and Ag single crystals exhibit an extended plateau in their CSS curves, indicating that the resolved shear stress, which promotes dislocation glide within the SB, is nearly constant over a wide plastic strain amplitude range. In addition, the cyclic saturation stress is much higher for the

Cu–Ag alloy, with the disappearance of the plateau in its CSS curve. Actually, cyclic saturation stress is even higher than in polycrystalline Cu with grain size 300–630 μm [53], though the microstructure of the Cu–Ag alloy is much coarser in the current study. Regarding the fatigue properties of Cu–Ag binary alloy, it is assumed that the development of long-range internal stresses may be the reason for cyclic hardening.

3.3. Slip morphologies and fatigue cracking

It is well known that when Cu single crystals are cyclically deformed, plastic deformation often concentrates in the form of SBs, with numerous extrusions appearing on the surfaces of the specimens [59,60]. For the Cu–Ag binary alloy, the SBs could pass continuously through the type II interface between the eutectic and dendrites (see Figures 3a and b), as they often have the same orientation or low misorientation angle. However, due to the presence of regions with different orientations inside the eutectic, the SBs could also be interrupted, coupled with the disappearance in certain regions of the eutectic (see Figure 3a). Such regions with disordered orientations should have higher yield strength, as expected from an extrapolation of the Hall–Petch relationship, resulting in the disappearance of SBs. While near the type I interface, SBs form large angles due to the high misorientation angles between the eutectic and dendrite (see Figures 3c and d). In Figure 3d, the SBs pass continuously through the eutectic and the upper dendrite, indicating that there is a type II interface between them. In addition, some SBs could also disappear in certain regions of the eutectic. From the CSS curve shown in Figure 2b, cyclic saturation stress increases with plastic strain amplitude; therefore, more SBs are prone to appear in the specimen surface as the plastic strain amplitude increases, with the apparent emergence of more slip patterns.

When the specimens were cyclically loaded at lower axial plastic strain amplitudes of 10^{-4} and 2.5×10^{-4} , the surface cracking morphologies are shown

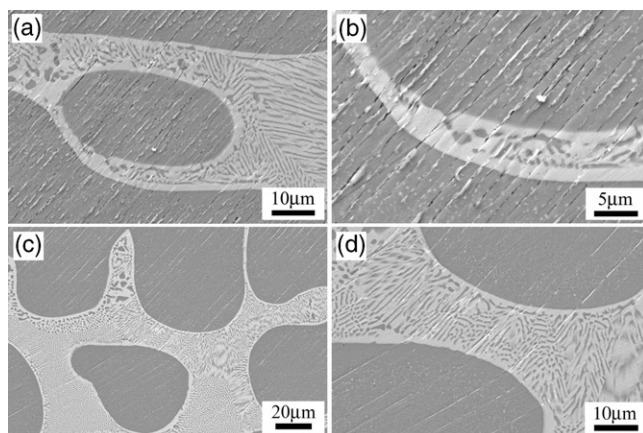


Figure 3. Surface slip morphologies in fatigued Cu–28wt%Ag alloy. (a,b) Slip morphologies near the type II interfaces ($\epsilon_{pl} = 5 \times 10^{-4}$, $N = 10^4$). (c,d) Slip morphologies near the type I interfaces ($\epsilon_{pl} = 10^{-4}$, $N = 2 \times 10^4$).

in Figure 4. Only severe extrusions and micro-cracks appear along the interphase interfaces (interphase interfaces inside the eutectic are excluded here) with loading up to 2×10^4 cycles under axial plastic strain amplitude of 10^{-4} (Figure 4a). With further cyclic deformation to fracture, fatigue cracks were also found along the interphase interfaces, as shown in Figure 4b. There is no SB in the eutectic region between the two micro-cracks; however, on both sides of this eutectic region, the slip directions of the two dendrites are identical; this cracking phenomena will be discussed in Section 4.1. When cyclically loaded at $\varepsilon_{pl} = 2.5 \times 10^{-4}$ for 1.5×10^4 cycles, the surface cracking sites are similar to those at $\varepsilon_{pl} = 10^{-4}$. It should be emphasized that the micro-cracks are along the type I interphase interfaces in Figures 4a and c. In Figure 4d, although the slip directions on both sides of the eutectic are identical, the SBs inside the eutectic are rather different, as illustrated inside the broken ellipse (see the faint slip traces), so, in this case, the cracking site is still considered a type I interface. The difference in orientation can be attributed to the nucleation of eutectic on a dendrite with another orientation [54].

When the specimen was cyclically loaded at $\varepsilon_{pl} = 5 \times 10^{-4}$, a larger number of SBs were activated; the surface cracking morphologies are shown in Figure 5. Both the interphase interfaces and SBs could be the preferred cracking sites, as occurred in pure Cu [19,20,61,62]. As seen in Figure 5c, there is some strain incompatibility in the interphase interface regions and some micro-cracks can also be found, as marked by the dotted line. With further cyclical loading to fracture, the fatigue cracks were found to propagate along the interphase interfaces and sometimes along the SBs (see Figure 5d).

Compared to the results above, fatigue cracking behavior became more complex when the Cu–Ag alloy was cyclically loaded at $\varepsilon_{pl} = 7.5 \times 10^{-4}$ for 5×10^3 cycles (Figure 6). Figures 6a and c show cracking sites along the type I interface and SBs,

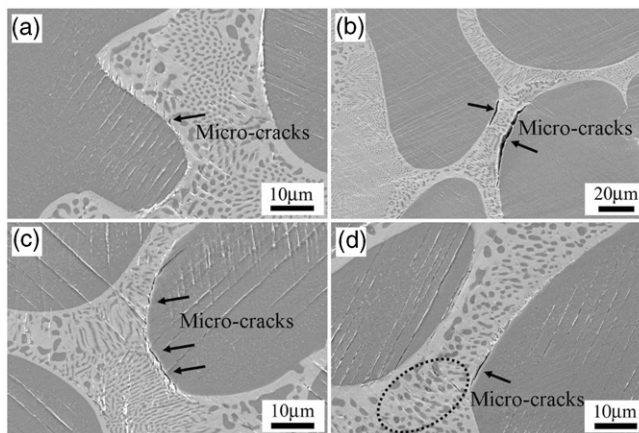


Figure 4. Fatigue cracking at low plastic amplitudes of 10^{-4} and 2.5×10^{-4} in fatigued Cu–28wt%Ag alloy: (a) along the type I interfaces ($\varepsilon_{pl} = 10^{-4}$, $N = 2 \times 10^4$); (b) along the interphase interfaces ($\varepsilon_{pl} = 10^{-4}$, loading to failure); (c) along the type I interface ($\varepsilon_{pl} = 2.5 \times 10^{-4}$, $N = 1.5 \times 10^4$); (d) along the interphase interfaces ($\varepsilon_{pl} = 2.5 \times 10^{-4}$, $N = 1.5 \times 10^4$).

respectively, which are similar to those observed at the plastic strain amplitudes described above. However, the cracking sites in Figure 6b are different, with the same slip direction on both sides of the eutectic, which is consistent with the observations in Figures 4b and d. In addition, a large number of deformation bands

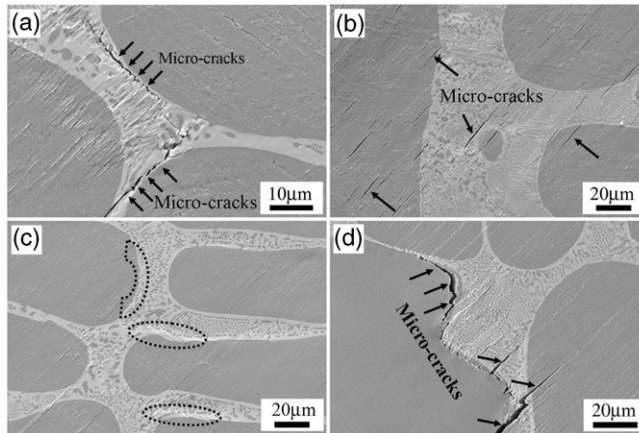


Figure 5. Fatigue cracking at plastic amplitude of 5×10^{-4} in fatigued Cu-28wt%Ag alloy: (a) along the type I interfaces ($N=10^4$); (b) along the SBs ($N=10^4$); (c) along the interphase interfaces ($N=10^4$); (d) along the interphase interfaces and along the SBs (loading to failure).

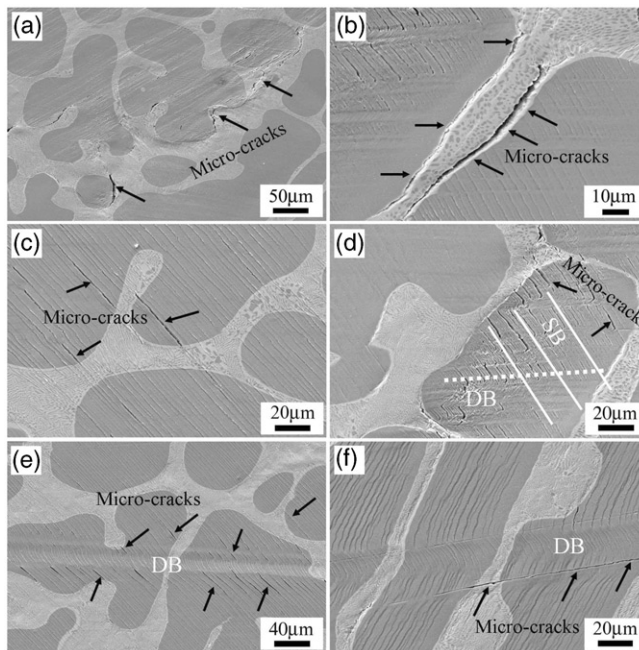


Figure 6. Fatigue cracking at plastic amplitude of 7.5×10^{-4} ($N=5 \times 10^3$) in fatigued Cu-28wt%Ag alloy: (a,b) along the interphase interfaces; (c-e) along the SBs; (f) along the DBs.

(DBs) appear and some micro-cracks initiate along the SBs just in front of the DBs (Figures 6d and e). Note the region where the cracks are just along the boundary of the DB, which is rather confusing (see Figure 6f), and will be discussed further in Section 4.2.

3.4. Fatigue fractography

To investigate the fatigue fracture surface, several specimens were cyclically deformed to failure. Figure 7 shows the fatigue fractographs of the specimen cyclically deformed at an axial plastic strain amplitude of 10^{-4} . The fracture surface is rather flat and three regions (regions A, B and C) with different features can be seen (Figure 7a). Since region C is the final fracture portion of the specimen, discussion on it is excluded here. Figures 7b and d, and Figures 7e and f show the fractographs of regions A and B, respectively. In macroscopic scale, no fatigue crack initiation site is obvious; however, from observation of the fatigue crack propagation direction, the upper left corner can be determined as the initiation site for fatigue cracking. In the early stage of fatigue crack propagation, some beach mark and tyre patterns can be clearly seen on the fractographs, as shown in Figures 7b and c, respectively. In addition, fatigue striations with spacing of ~ 300 nm were also found in region A, as shown in Figure 7d, indicating steady propagation of the fatigue crack. In the late stage of cyclic deformation, Figure 7e shows the fatigue striations in

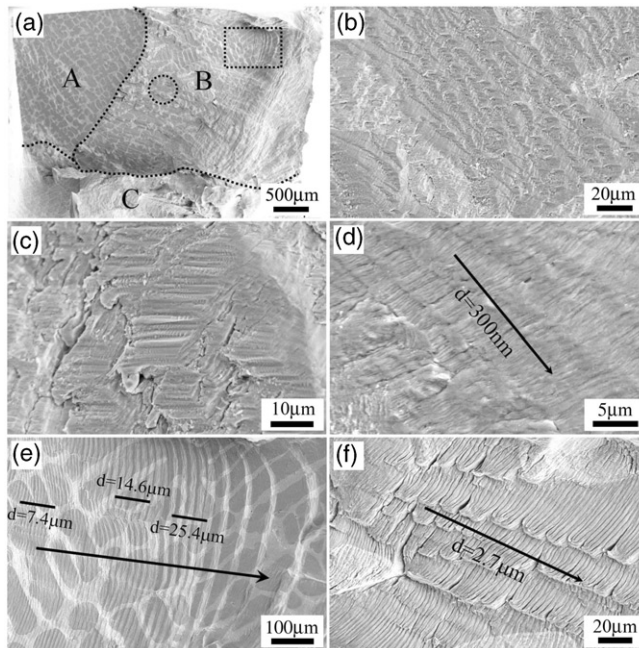


Figure 7. (a) Fatigue fracture surface of Cu-28wt%Ag alloy at $\varepsilon_{pl} = 10^{-4}$. (b-d) Fracture morphologies in region A. (e,f) Fracture morphologies in region B.

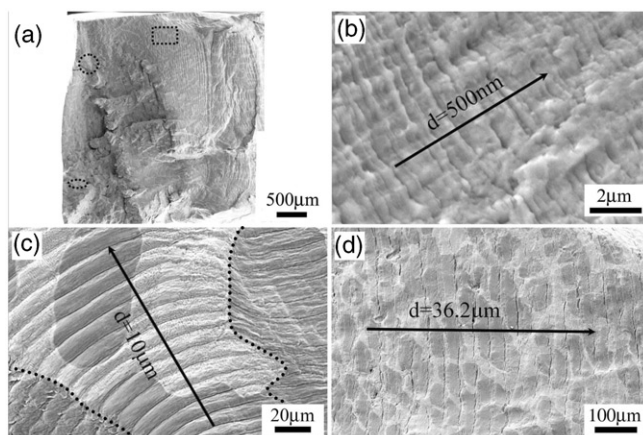


Figure 8. (a) Fatigue fracture surface of Cu-28wt%Ag alloy at $\varepsilon_{pl} = 5 \times 10^{-4}$. (b-d) Fracture morphologies in (a), as indicated by the ellipse, circle and rectangle, respectively.

region B, as indicated by the rectangle in Figure 7a, with striation spacing labeled in different regions and the arrow representing the fatigue crack propagation direction. Striation spacing increases significantly with cyclic deformation. Figure 7f, as indicated by the circle in Figure 7a, shows that the fracture surface in region B consists of numerous well-defined fatigue striations, with spacing of $\sim 2.7 \mu\text{m}$. In addition, secondary cracks along the striations are also found. From the fatigue fractographic observations above, it is worth noting that the eutectic shows no impediment to fatigue crack propagation. This is consistent with the results of surface slip morphologies, as presented in Section 3.3.

Figure 8 shows fatigue fractographs of the specimen cyclically deformed at an axial plastic strain amplitude of 5×10^{-4} . Similar to Figure 7, fatigue striations are also found on the fracture surface. As indicated by the ellipse, circle and rectangle in Figure 8a, Figures 8b-d show the fracture morphologies in different regions, respectively, with striation spacings and fatigue crack propagation directions labeled. Fatigue striations are larger and secondary cracks along the striations are more common, in contrast to the specimen cyclically deformed at an axial plastic strain amplitude of 10^{-4} . As shown in Figure 8c, the striations can cross the interfaces between the eutectic and dendrites, which are type II interfaces. In contrast, the dot lines represent the type I interfaces, as the striations are different near the interfaces. Observations of the fatigue fracture surfaces suggest that the fatigue striations are the consequence of successive rounding and sharpening of the crack tip at each cycle [63]. On the other hand, during the crack propagation process, the intense stress concentrated near the crack tip may play an important role in accelerating secondary cracking along the striations.

4. Discussion

It is recognized that, in fcc metals, typical fatigue cracking are either along PSBs or GBs or both in single or polycrystalline materials [17-20,61,62]. To date, the widely

accepted models for the two typical fatigue cracking modes are the extrusion–intrusion mechanism [14–16] and the PSB–GB (or piling-up of dislocations) mechanism [23]. Based on the PSB–GB mechanism, Zhang et al. [24,25] explained the cracking phenomena of Cu bicrystals as follows: fatigue cracking always occurs along the high-angle GBs, irrespective of the interaction angle between the GB plane and the loading direction; in contrast, for the columnar crystals containing low-angle GBs, fatigue crack preferentially initiates along PSBs rather than along the low-angle GBs. In multi-phase alloys, interphase interfaces are frequently observed to be the preferential cracking sites. For example, in 304L stainless steels, fatigue crack initiation at the δ -ferrite/ γ phase interface is attributed to strain incompatibility [64], whereas in SA333 plain carbon steel containing ferrite and pearlite, elastic–plastic incompatibility is suggested to be the primary mechanism for crack initiation at the ferrite–pearlite interfaces [65]. For Ti-6242 alloy with duplex phases, it was found that crack initiation occurs by coalescence of shear-induced cavities nucleated at α/β interfaces [40].

For the Cu–28wt%Ag binary alloy in this study, the typical fatigue cracking sites are mainly along the interphase interfaces or along SBs. Note that, though the fraction of the interphase interfaces is rather high, only a few of them are preferential sites for fatigue cracking. Conversely, most still retain their original morphology, without any preliminary crack or strain incompatibility. The insensitivity of the interphase interfaces to fatigue cracking is believed to be largely related to its microstructure. For fatigue cracking along SBs, it is generally accepted that the mechanism can be explained by the surface roughness model based on annihilation of dislocations inside the SBs [15]. In the following sections, mechanisms of fatigue cracking along interphase interfaces and DBs will be discussed.

4.1. Fatigue cracking along interphase interfaces

In contrast to the multi-phase alloys discussed above, Cu–28wt%Ag binary alloy contains two ductile phases with an fcc structure and both phases have some orientation relationship, which may play an important role in cyclic deformation, especially in fatigue damage behavior. In this study, fatigue cracks were observed to nucleate only along a few of the interphase interfaces (see Figure 9a). In most cases, there is no fatigue cracking along the interphase interfaces, indicating a strong resistance to the interfacial damage. Thus, the microstructure of the Cu–Ag alloy differs greatly from the hypoeutectic Al–Si alloys, duplex Ti alloys and steels [35–42,64,65], which have two phases with different crystal structures. As a result, the fatigue damage mechanism of Cu–Ag alloy should be very different. Based on the classification of the interphase interfaces outlined in Section 3.1, i.e. type I and type II interface, their corresponding fatigue mechanisms will be discussed as follows.

During cyclic deformation of fcc materials, it is known that most of the plastic strains are carried by SBs [59,60] and the SBs may become carriers and channels to transport the dislocations and vacancies from the grain interiors to the GBs. Using the ECC technique in SEM, Zhang et al. [24,25] investigated the interactions between PSBs with GBs in various Cu bicrystals. They found that, in columnar crystals

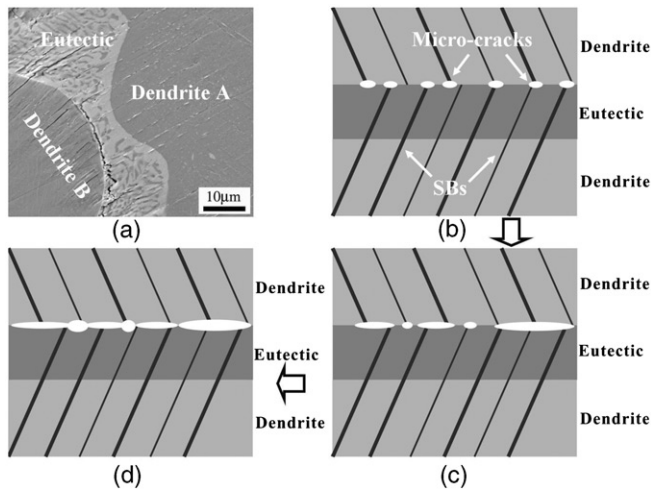


Figure 9. (a) Fatigue cracking along the interphase interface ($\epsilon_{pl} = 5 \times 10^{-4}$, $N = 10^4$). (b–d) Cracking mechanism along the interphase interface.

containing low-angle GBs, dislocations carried by PSBs can pass continuously through the low-angle GBs, and no cracks were found along the GBs. In bicrystals containing high-angle GBs, on the other hand, dislocations are prone to pile up at the GBs, which are always the preferential cracking sites. Figure 9a clearly shows that the SBs in dendrite A can pass continuously through the eutectic, but terminate just before reaching dendrite B. Thus, the interphase interface between the eutectic and dendrite A is considered to be a type II interface, whereas the interphase interface between the eutectic and dendrite B is a type I interface. Here, it seems that the type II interface shows little impediment to the continuity of the SBs. This is understandable because the preeutectic dendrite may act as the nuclei of the eutectic [54]; thus, in subsequent solidification, the eutectic will keep the same orientation or low misorientation angle with the dendrites (see Figure 1b) and, as a result, the same crystal structure and coplanar slip systems make it easy to slip continuously through the eutectic and the dendrite. As shown in Figure 9a, during cyclic push–pull loading, it is assumed that dislocations carried by SBs can be transported continuously through the type II interface between the eutectic and dendrite A. What is more, the fatigue cracks are just located along the intersecting plane between dendrite B and the eutectic, which is a type I interface containing high misorientation angle. The cracking mechanism can be explained as follows: dislocations carried by SBs will terminate and be piled up at the interface; with further cyclic deformation, more and more residual dislocations are piled up and, as a result, some micro-cracks gradually appear in different sites of the interface (see Figure 9b). Micro-cracks subsequently propagate by their linking up (see Figure 9c). Finally, when the micro-cracks conjoin with each other, bigger cracks appear (see Figure 9d). It is emphasized that some special cracks are also found along the interphase interfaces (see Figures 4b, d and Figure 6b), which is supposed to be the result of strain incompatibility near the interface, because the eutectic has an orientation different from that of the dendrite.

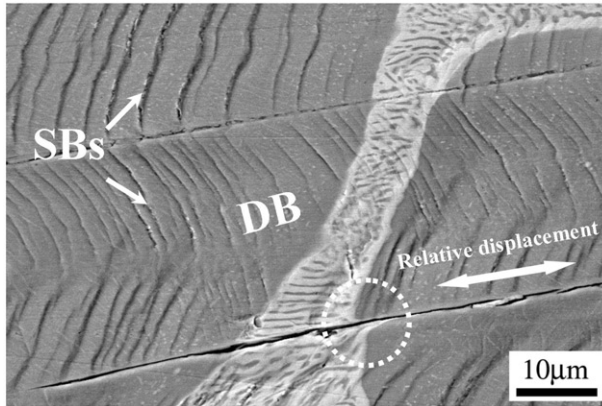


Figure 10. Fatigue cracking along DB ($\epsilon_{pl} = 7.5 \times 10^{-4}$, $N = 5 \times 10^3$).

The appearance of this eutectic may be resulted of nucleation on another dendrite with a different orientation [54].

4.2. Fatigue cracking along DBs

During the cyclic loading process, DBs were also observed when the applied plastic strain amplitude was high, e.g. $\epsilon_{pl} = 7.5 \times 10^{-4}$. It is of interest that an extraordinary cracking site exists along the DB, as illustrated in Figure 10 (the same region as in Figure 6f). It is apparent that, in the interior of the DB, some SBs appear and the slip plane differs from that in the surrounding area. In addition, they are significantly curved. Inside the circle, the eutectic was slightly elongated, and the eutectic above and below the crack was staggered, implying that the DB had a relative displacement and the orientation inside the DB changed in contrast to the surrounding matrix; thus, the SBs lost continuity and the one-to-one relationship. Zhang et al. [66] reported that, in Cu single crystals, the formation of DBs often induced crystal rotation when shearing occurred on the $(\bar{1}01)$ plane and, with further cyclic deformation, shear irreversibility resulted in surface roughness, which finally led to fatigue cracking within DBs. Thus, it is understandable that fatigue cracks occurring along DB should result from the appearance of discontinuous interfaces between DBs and the matrix.

In most cases, however, fatigue cracking did not occur along the DBs. Figures 11a and b show two types of DB, with some fatigue cracks along the SBs that are just in front of the DB. In addition, it appears that the DB in Figure 11b is much wider than that in Figure 11a. Assuming that there are more plastic strains trapped in the narrow DB, it should play a much more important role in interrupting the continuity of the SBs. Actually, in contrast to Figure 11b, more fatigue cracks were found in Figure 11a. Due to the existence of a shear stress along the DB, namely, a relative displacement along the DB (see Figure 10), this will play an important role in tearing the SBs to form the crack (see Figures 11a and b) when cyclic deformation is carried out and the interface between the SB and matrix becomes sufficiently weak. As shown in Figure 11c, when the displacement direction

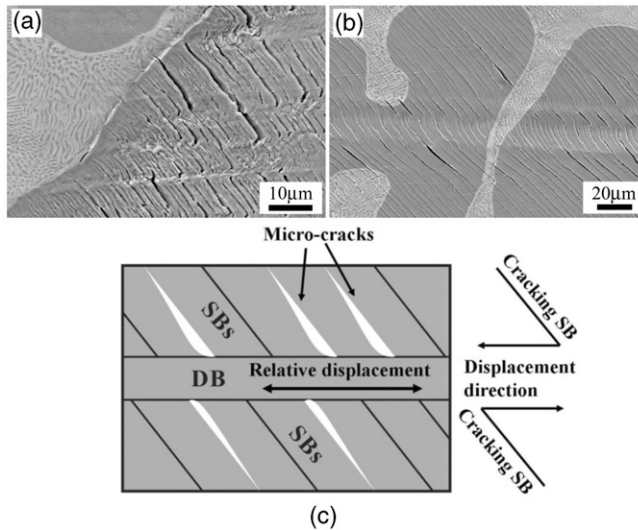


Figure 11. (a,b) Fatigue cracking along SBs that are in front of DB ($\epsilon_{pl} = 7.5 \times 10^{-4}$, $N = 5 \times 10^3$). (c) Illustration of effect of DB on fatigue cracking along SBs.

of the DB is towards the left, a shear stress will be exerted on the upper SBs along the left direction, resulting in cracking within them; while the shear stress towards the right will cause fatigue cracking in the lower SBs. Since cyclic deformation is controlled under push–pull loading, the shear stress will be exerted on the SBs alternately to form fatigue cracking in the upper and lower SBs.

5. Conclusions

Based on observations of cyclic deformation and fatigue damage behavior in Cu–28wt%Ag binary alloy, the following conclusions can be drawn:

- (1) The initial cyclic hardening stage of Cu–28wt%Ag alloy is short (<100 cycles), which differs from that of pure Cu single crystals or polycrystals. Cyclic saturation stress monotonically increases with increasing strain amplitude.
- (2) Near the type II interface, the eutectic and dendrite often have the same orientation or low misorientation angle. Thus, it is proposed that the reason for the non-cracking behavior of the interphase interfaces is that the dislocations carried by SBs can be continuously transported through the interface during cyclic push–pull loading, without piling-up of dislocations at the type II interface.
- (3) Fatigue striations appear on the fatigue fracture surface and secondary cracking occurs along the fatigue striations. The spacing of the striations becomes wider and secondary cracks along the striations are more prone to occur at higher plastic strain amplitude. In addition, the eutectic shows little or no impediment to fatigue crack propagation.

- (4) Fatigue cracks along the SBs and the type I interface are always observed. DBs appear at higher plastic strain amplitude. For type I interfaces, the cracking behavior along them can be explained by the PSB–GB damage mechanism.

Acknowledgements

The authors thank Q.Q. Duan, P. Li, H.J. Yang, W. Gao, H.H. Su, J.L. Wen and G. Yao for sample preparation, mechanical tests and SEM observations. This work was financially supported by the “Hundred of Talents Project” of Chinese Academy of Sciences, and the National Natural Science Foundation of China (NSFC) under grant Nos. 50571104, 50625103 and 50890173.

References

- [1] J.A. Ewing and J.C. Humfrey, *Phil. Trans. R. Soc. A* 200 (1903) p.241.
[2] N. Thompson, N. Wadsworth and N. Louat, *Phil. Mag.* 1 (1956) p.113.
[3] J.F. Finney and C. Laird, *Phil. Mag.* 31 (1975) p.339.
[4] A.S. Cheng and C. Laird, *Fatigue Eng. Mater. Struct.* 4 (1981) p.331.
[5] J. Polák, *Mater. Sci. Eng.* 92 (1987) p.71.
[6] J. Polák, T. Lepistö and P. Kettunen, *Mater. Sci. Eng.* 74 (1985) p.85.
[7] P. Lukáš and L. Kunz, *Mater. Sci. Eng. A* 314 (2001) p.85.
[8] L.M. Brown, *Mater. Sci. Eng. A* 285 (2000) p.35.
[9] Z.S. Basinski and S.J. Basinski, *Scripta Metall.* 18 (1984) p.851.
[10] Z.S. Basinski and S.J. Basinski, *Acta Metall.* 33 (1985) p.1307.
[11] Z.S. Basinski and S.J. Basinski, *Acta Metall.* 33 (1985) p.1319.
[12] Z.S. Basinski and S.J. Basinski, *Acta Metall.* 37 (1989) p.3263.
[13] A. Hunsche and P. Neumann, *Acta Metall.* 34 (1986) p.207.
[14] U. Essmann and H. Mughrabi, *Phil. Mag. A* 40 (1979) p.731.
[15] U. Essmann, U. Gösele and H. Mughrabi, *Phil. Mag. A* 44 (1981) p.405.
[16] K. Differt, U. Essmann and H. Mughrabi, *Phil. Mag. A* 54 (1986) p.237.
[17] J.C. Figueroa and C. Laird, *Mater. Sci. Eng.* 60 (1983) p.45.
[18] H. Mughrabi and R. Wang, in *Defects, fatigue and fracture*, G.C. Sih and H. Zorski, eds., Martinus Nijhoff, The Hague, 1982, p.15.
[19] C.V. Cooper and M.E. Fine, in *Defects, fatigue and fracture*, G.C. Sih and H. Zorski, eds., Martinus Nijhoff, The Hague, 1982, p.183.
[20] G.H. Kim, I.B. Kwon and M.E. Fine, *Mater. Sci. Eng. A* 142 (1991) p.177.
[21] W.H. Kim and C. Laird, *Acta Metall.* 26 (1978) p.777.
[22] W.H. Kim and C. Laird, *Acta Metall.* 26 (1978) p.789.
[23] H. Mughrabi, F. Ackermann and K. Herz, *ASTM STP* 811 (1983) p.5.
[24] Z.F. Zhang and Z.G. Wang, *Prog. Mater. Sci.* 53 (2008) p.1025.
[25] Z.F. Zhang and Z.G. Wang, *Acta Mater.* 51 (2003) p.347.
[26] Z.F. Zhang and Z.G. Wang, *Phil. Mag. A* 79 (1999) p.741.
[27] Z.F. Zhang and Z.G. Wang, *Phil. Mag. A* 81 (2001) p.399.
[28] Z.F. Zhang and Z.G. Wang, *Phil. Mag. Lett.* 80 (2000) p.483.
[29] Z.F. Zhang, Z.G. Wang and Y.M. Hu, *Mater. Sci. Eng. A* 272 (1999) p.410.
[30] J. Polák, J. Man and K. Obrtlík, *Int. J. Fatigue* 25 (2003) p.1027.
[31] J. Polák, *Mater. Sci. Eng. A* 468/470 (2007) p.33.
[32] C. Déprés, C.F. Robertson and M.C. Fivel, *Phil. Mag.* 86 (2006) p.79.

- [33] M. Risbet, X. Feugas, C. Guillemer-Neel and M. Clavel, *Scripta Mater.* 49 (2003) p.533.
- [34] M. Risbet and X. Feugas, *Eng. Fract. Mech.* 75 (2008) p.3511.
- [35] J. Stolarz, O. Madelaine-Dupuich and T. Magnin, *Mater. Sci. Eng. A* 299 (2001) p.175.
- [36] S. Ankem, H. Margolin, C.A. Greene, B.W. Neuberger and P.G. Oberson, *Prog. Mater. Sci.* 51 (2006) p.632.
- [37] Y. Saleh and H. Margolin, *Metall. Trans. A* 14 (1983) p.1481.
- [38] X. Demulsant and J. Mendez, *Mater. Sci. Eng. A* 219 (1996) p.202.
- [39] J. Mendez, *Mater. Sci. Eng. A* 263 (1999) p.187.
- [40] P. Lefranc, V. Doquet, M. Gerland and C. Sarrazin-Baudoux, *Acta Mater.* 56 (2008) p.4450.
- [41] Y. Motoyashiki, A. Brückner-Foitt and A. Sugeta, *Eng. Fract. Mech.* 75 (2008) p.768.
- [42] I. Alvarez-Armas, M.C. Marinelli, J.A. Malarria, S. Degallaix and A.F. Armas, *Int. J. Fatigue* 29 (2007) p.758.
- [43] A. Pineau and R. Pelloux., *Metall. Trans. A* 5 (1974) p.1103.
- [44] V. Calonne and A. Gourgues, A. Pineau, *Fatigue Fract. Eng. Mater. Struct.* 27 (2004) p.31.
- [45] Y. Sakai and H.-J. Schneider-Muntau, *Acta Mater.* 45 (1997) p.1017.
- [46] K. Han, A.A. Vasquez, Y. Xin and P.N. Kalu, *Acta Mater.* 51 (2003) p.767.
- [47] W. Grünberger, M. Heilmaier and L. Schultz, *Z. Metallkd.* 93 (2002) p.58.
- [48] D. Dew-Hughes, *Mater. Sci. Eng. A* 168 (1993) p.35.
- [49] J.T. Wood, J.D. Embury and M. Ashby, *Acta Mater.* 45 (1997) p.1099.
- [50] P.H. Frings and L. Van Bockstal, *Physica B* 211 (1995) p.73.
- [51] J. Freudenberger, H.-J. Klaufß, K. Heinze, A. Gaganov, M. Schaper and L. Schultz, *Int. J. Fatigue* 30 (2008) p.437.
- [52] S. Qu, P. Zhang, S.D. Wu, Q.S. Zang and Z.F. Zhang, *Scripta Mater.* 59 (2008) p.1131.
- [53] P. Zhang, Q.Q. Duan, S.X. Li and Z.F. Zhang, *Phil. Mag.* 88 (2008) p.2487.
- [54] Y.Z. Tian and Z.F. Zhang, *Mater. Sci. Eng. A* 508 (2009) p.209.
- [55] K. Nogita and A.K. Dahle, *Mater. Character.* 46 (2001) p.305.
- [56] P. Li, Z.F. Zhang, S.X. Li and Z.G. Wang, *Acta Mater.* 56 (2008) p.2212.
- [57] H. Mughrabi, *Mater. Sci. Eng.* 33 (1978) p.207.
- [58] P. Li, Z.F. Zhang, S.X. Li, Z.G. Wang, *Phil. Mag.* (2009), under review.
- [59] T. Luoh and C.P. Chang, *Acta Mater.* 44 (1996) p.2683.
- [60] R. Zauter, F. Petry, M. Bayerlein, C. Sommer, H.-J. Christ and H. Mughrabi, *Phil. Mag. A* 66 (1992) p.425.
- [61] B.T. Ma and C. Laird, *Acta Metall.* 37 (1989) p.325.
- [62] B.T. Ma and C. Laird, *Acta Metall.* 37 (1989) p.337.
- [63] C. Laird and G.C. Smith, *Phil. Mag.* 7 (1962) p.847.
- [64] B.S. Rho, H.U. Hong and S.W. Nam, *Int. J. Fatigue* 22 (2000) p.683.
- [65] N. Narasaiah and K.K. Ray, *Mater. Sci. Eng. A* 474 (2008) p.48.
- [66] Z.F. Zhang, Z.G. Wang and Z.M. Sun, *Acta Mater.* 49 (2001) p.2875.